

The nature of synchronisation in power systems: inspirations from communication systems

Yunjie Gu^{1,2}, Yitong Li¹, Timothy C. Green¹

¹Imperial College London, London, UK. ²University of Bath, Bath, UK.

The large-scale integration of converter-interfaced resources in electrical power systems raises new threats to stability which call for new theoretic frameworks for modelling and analysis. Here we present the theory of power-communication isomorphism to as a step to address this grand challenge. It is revealed that an intrinsic communication mechanism governs the synchronisation of all apparatuses in power systems based on which a unified representation for heterogeneous apparatus and behaviours is established. This new theory yields a simple stability criterion for complex systems that can be intuitively interpreted and thus conveniently applied in practice. We also demonstrate that a system of 100% converter-interfaced resources can be well stabilised under grid-following control which was commonly considered impossible.

Driven by the imperative of decarbonisation and clean growth, the primary energy of power systems is transforming from fossil fuels to renewable resources. The change of the primary energy is accompanied by the change of technologies for power generation and conversion. Renewable resources, mainly wind and solar energy, as well as grid-scale battery storage plants, are interfaced to power systems by power electronic converters instead of conventional synchronous generators. The increasing penetration of converter-interfaced resources poses new threats to system stability. Converter-induced oscillations have been reported worldwide, many of which had major consequences. For example, the 2019 power outage in UK was, in part, triggered by the sub-synchronous oscillation of wind turbine converters in Hornsea wind farms according to report provided by National Grid UK [1]. Such converter-induced oscillation phenomena are beyond the prediction of state-of-the-art stability models and the underpinning mechanisms are not fully understood, which have drawn international attention.

The stability of a power system is defined as the ability to keep all apparatus in the system synchronised to a single frequency with expected power flows and voltage profiles throughout the system [2], [3]. The classic stability theory for power systems is tailor-made for synchronous generators which are governed by the physical law of the motion of rotors. However, converters are governed by control algorithms, which gives rise to almost infinite flexibility, and therefore complexity, in converter behaviours [4]. New synchronisation and power control schemes have been developed for converters to serve different design targets, such as reducing the size of power devices and mitigating harmonic distortion. The design targets are oriented to local concerns whereas the system-level impacts of these new schemes are unclear. It is extremely difficult to establish a single generic model for system studies that represents the wide variety of control-defined behaviours. State-of-the-art studies on converter-induced instabilities have been limited to specific cases and there have been no generic conclusions given nor consensus reached [5], [6].

To address this challenge, we looked again at the nature of power systems and revealed that there is an intrinsic communication mechanism underlying power systems, which we describe as a power-communication isomorphism. This isomor-

phism governs the synchronisation in power systems upon which a unified representation for heterogeneous apparatuses and behaviours is established. This new theory creates new insights into power system dynamics and yields new stability criteria that can be applied systematically. We also demonstrate that a power system with nearly 100% converter-interfaced resources under grid-following control can be well stabilised over various transients, provided that the control parameters are properly designed under the guidance of our new theory. This was commonly considered impossible in state-of-the-art models, and is a surprising and valuable result from the new theory.

Power-Communication Isomorphism

The concept of power-communication isomorphism is illustrated in Fig. 1. The voltages and currents in a power system are seen as communication signals carrying both energy and information. The power apparatuses, including generators and converters, serve as modulators in that they create three-phase sinusoidal signals from internal oscillators (or rotors). The amplitude, frequency and phase of an internal oscillator are baseband signals which are shifted to the carrier-band of 50 Hz or 60 Hz via frame transformation or rotation, creating an effect equivalent to amplitude-angle modulation. Mathematically, a three-phase signal is represented as a complex number $Ae^{j\theta}$, where A and θ are the amplitude and angle of the signal [7], [8]. The amplitude and angle can be combined into a complex phase defined as $\vartheta = \ln A + j\theta$, so the amplitude-angle modulation can be jointly expressed as a complex exponential function

$$e^{j\vartheta} = Ae^{j\theta} = A(\sin \theta + j \cos \theta) \quad (1)$$

The time-derivative of the ϑ is called the complex frequency $\varpi = \dot{\vartheta} = A^{-1}\dot{A} + j\omega$, whose real part reflects amplitude variation, and the imaginary part $\omega = \dot{\theta}$ is the angular frequency.

The modulated signals are propagated over a power network that can be viewed as communication channels. The channels include all passive components in the power network, including transmission lines, transformers, series/shunt compensators, harmonic filters, and passive loads. The active apparatuses, including generators and converters, are defined as nodes that interact (communicate) over the channels. There are two types of nodes in a power system, namely voltage nodes (representing grid-forming apparatuses, including synchronous generators and

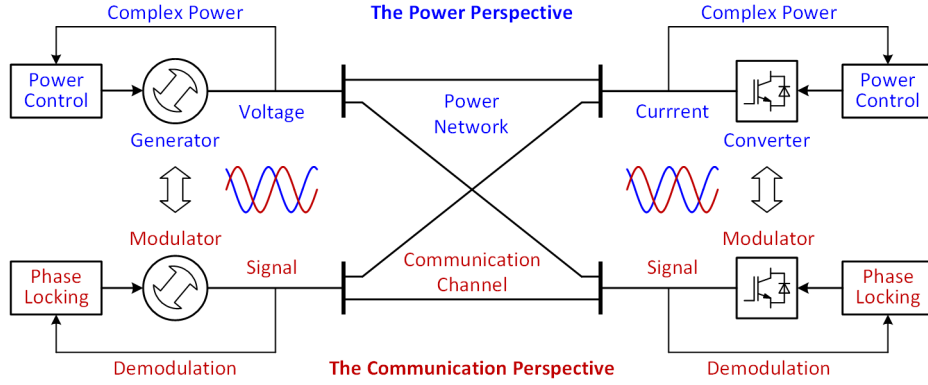


Fig. 1. Illustration of power-communication isomorphism in power systems. The upper part shows a part of system viewed from the perspective of power flow and the lower part is viewed from the perspective of communication.

grid-forming converters) and current nodes (representing grid-following converters) [4], [9]. A voltage node transmits a voltage signal to the network and receives a current signal, and a current node does the opposite. For either cases, the complex power seen at a node is defined as [10]

$$S = e^{\vartheta_{\text{tx}}} e^{\vartheta_{\text{tx}}^*} = A_{\text{tx}} A_{\text{rx}} e^{j(\theta_{\text{rx}} - \theta_{\text{tx}})} \quad (2)$$

where $e^{\vartheta_{\text{tx}}}$ is the transmitted signal, $e^{\vartheta_{\text{rx}}}$ is the received signal, and the superscript * denotes complex conjugation. There may be multiple nodes in the network and their signals are received as a single signal at each node by superposition. The alternating parts of $e^{\vartheta_{\text{tx}}}$ and $e^{\vartheta_{\text{rx}}}$ are cancelled in the complex conjugation which means that the complex power has a demodulation effect that transforms a carrier-band signal back to base-band. The argument of S is exactly the angle difference $\theta_{\text{rx}} - \theta_{\text{tx}}$, implying that the control of complex powers is isomorphic to the phase-locking of signals.

Mathematical Description

Despite the power-communication isomorphism, there are significant differences between a power system and a communication system. Firstly, the carrier frequency in a communication system is constant. In contrast, the carrier frequency in a power system is time-varying due to load fluctuation, especially in a converter-based power system with reduced rotation inertia. Secondly, the signals in a communication system are usually narrow-band signals and the corresponding channel has a flat frequency response, meaning that the channel distortion can be neglected or mitigated by equalisation [11]. The signals in a power system, however, may be wide-band signals (especially during the transients after faults), and the channel distortion is no longer negligible [2]. Thirdly, a communication system usually has two-way interaction but a power system has multi-way interaction. For example, for a cellular network, two devices communicate indirectly via the base station and the inter-device cross-talk is eliminated by various multiplexing technologies [12]. In contrast, the apparatuses in a power system have overlapped bandwidths with no multiplexing at all, resulting in more entangled and hence complicated interaction patterns. A new mathematical description is needed to reconcile these significant differences and thus establish the power-communication isomorphism rigorously, which we present below.

A channel is a linear system that can be represented as a transfer function $G(s)$ in the frequency domain. Since the modulation-demodulation has a frequency shifting effect, the equivalent transfer function seen by the base-band signals is shifted to $G(j\omega_c + s)$ according to Fourier analysis [13]. This frequency shift representation assumes a constant carrier frequency which does not hold for a power system, as discussed above. To address this issue, we propose a new time-domain representation for a channel. Define the time-domain gain of a channel as $g = e^{\hat{\vartheta}}/e^{\vartheta}$ where e^{ϑ} and $e^{\hat{\vartheta}}$ are the input and output signals of the channel respectively. The alternating part of e^{ϑ} and $e^{\hat{\vartheta}}$ are cancelled in the division so g is a base-band variable. We will transform the dynamics of signals to the dynamics of g and show that g is shaped by the complex frequency ϖ of the input signal e^{ϑ} . $G(s)$ can be decomposed into a series of first-order systems $G(s) = \sum_k (s - \lambda_k)^{-1} \zeta_k$, each of which induces a gain g_k , and the total gain is the sum of all g_k . We simply investigate one of the first-order systems $G(s) = (s - \lambda)^{-1} \zeta$ without losing generality, where λ is the eigenvalue of the system and ζ is the input gain. The corresponding differential equation for modulated signals is

$$d e^{\hat{\vartheta}}/dt = \lambda e^{\hat{\vartheta}} + \zeta e^{\vartheta} \quad (3)$$

which yields the differential equation for the channel gain g

$$dg/dt = (\lambda - \varpi)g + \zeta. \quad (4)$$

It is clear that g depends on ϖ dynamically, and this effect is named *dynamic frequency shift* as an extension to the (static) frequency shift in Fourier analysis. It is worth noting that the dynamics of g is non-linear although the channel is linear.

Taking into account the channel gain, the overall model for the power-communication isomorphic system is illustrated in Fig. 2. For a network with N nodes, the n -th node transmits a signal e^{ϑ_n} to the network which is demodulated by another node m to yield $\hat{S}_{mn} = e^{\vartheta_n} e^{\vartheta_m^*}$. We put $\hat{\cdot}$ on \hat{S}_{mn} because it is not physical power as the channel gain is not yet included. Considering the channel gain, the complex power transfer over the channel from the n -th node to the m -th node is $S_{mn} = g_{mn} \hat{S}_{mn}$ where g_{mn} is the corresponding channel gain. All traffics in the network share the channels according to the superposition principle, so the total complex power received at node m is the summation of $S_m = \sum_n S_{mn}$. The total complex power S_m

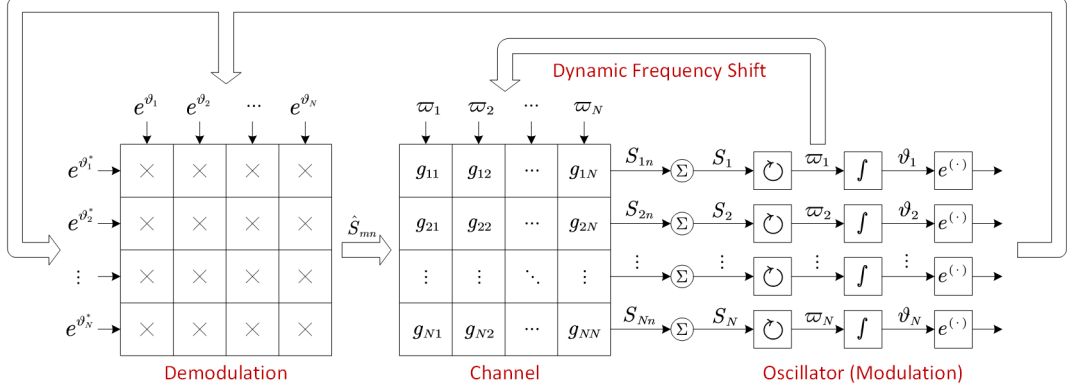


Fig. 2. Illustration of the mathematical description for a power-communication isomorphic system. Symbols: $*$ denotes complex conjugation, \times denotes multiplication, \sum denotes summation, \circlearrowright denotes complex frequency synthesising, and \int denotes integration.

is fed to the oscillator of the m -th node. The oscillator synthesises the internal complex frequency ϖ_m and complex angle ϑ_m , from which the signal e^{ϑ_m} is generated and transmitted to channels, and thus closes the loop of modulation-demodulation.

The dynamic frequency shift reveals interesting properties of base-band signal propagation over a channel. We solve g from (4) and put it into S_{mn} . To address the non-linearity of g -dynamics, we linearise the solution by perturbation

$$\Delta S_{mn} = S_{mn0}(\Delta\vartheta_m^* + F \cdot \Delta\vartheta_n) \quad (5)$$

where the prefix Δ and subscript 0 denote the perturbation and equilibrium of a dynamic variable, and F is a low pass filter

$$F(s) = \frac{j\omega_0 - \lambda}{s + j\omega_0 - \lambda}. \quad (6)$$

It is clear from (5) that a channel induces asymmetry in base-band signal propagation. The angle perturbation $\Delta\vartheta_m$ at the receiving end m affects the complex power ΔS_{mn} instantaneously, whereas the angle perturbation $\Delta\vartheta_n$ at the transmitting end n passes through a low-pass filter F before affecting ΔS_{mn} . Thus F characterise the dynamic property of the channel and we defined the *channel bandwidth* as

$$\begin{aligned} \omega_b &= \sup |\omega|, \text{ subject to} \\ |F(j\omega)| &> 1/\sqrt{2} \text{ and } |\angle F(j\omega)| < \pi/4. \end{aligned} \quad (7)$$

The channel bandwidth sets the limit speed of power-angle propagation on the channel. The wide-band signals beyond the channel bandwidth decay over channels or induce excessive phase delays, and this have significant impact on power system stability, as we will discuss in the next section. Within the channel bandwidth, the channel gain g responds almost instantaneously to ϖ . In such a case, g can be approximately solved by letting $dg/dt = 0$ in (4) which yields

$$g \approx (\varpi - \lambda)^{-1} \zeta = G(\varpi). \quad (8)$$

Unified Synchronisation Principle

As illustrated above, the signal of each apparatus is generated by the internal oscillator. The stability of a power system is thus reformulated as the ability of all oscillators to synchronise and yield the expected signal-power flow across the network.

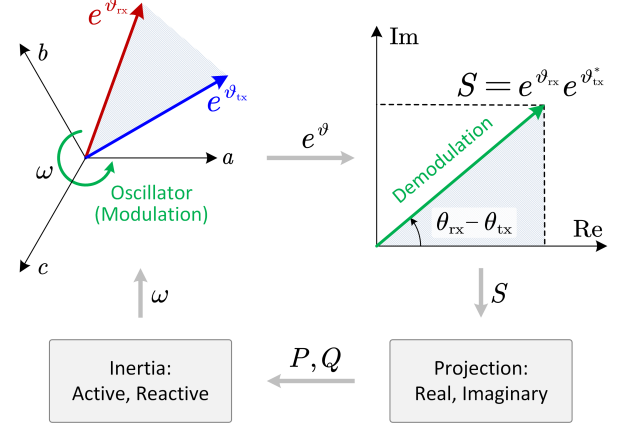


Fig. 3. Unified synchronisation principle in the light of power-communication isomorphism. The rotor and PLL of voltage nodes (grid-forming) and current nodes (grid-following) are equivalent to real and reactive inertia respectively.

Synchronisation is an essential reflection and arguably the cornerstone of power system stability. There are heterogeneous synchronisation schemes co-existing in power systems which present an obstacle for systemic analysis. Voltage nodes use power-based synchronisation via physical or emulated rotors [14], [15], whereas current nodes use signal-based synchronisation via phase-locked loops (PLLs). The theory of power-communication isomorphism reveals the unified principle underlying the power- and signal-based synchronisation schemes.

As illustrated in Fig. 3, the demodulated complex power S is projected onto either the real or imaginary axis to yield the active or reactive power (P or Q). Either P or Q may serve as a detector of the angle difference $\theta_{rx} - \theta_{tx}$, which is fed into the internal oscillator to control its angular velocity ω and thus keep the angle difference at an expected value via negative feedback. The oscillator maps the active or reactive power to the acceleration/deceleration of ω and therefore has an equivalent effect to an inertia. The projection onto the real axis (P) corresponds to the power-based synchronisation (rotor) of voltage nodes (grid-forming). The projection onto the imaginary axis (Q) corresponds to the signal-based synchronisation (PLL) of current nodes (grid-following). The inertia associated to P and Q is active and reactive inertia respectively. Thus we establish

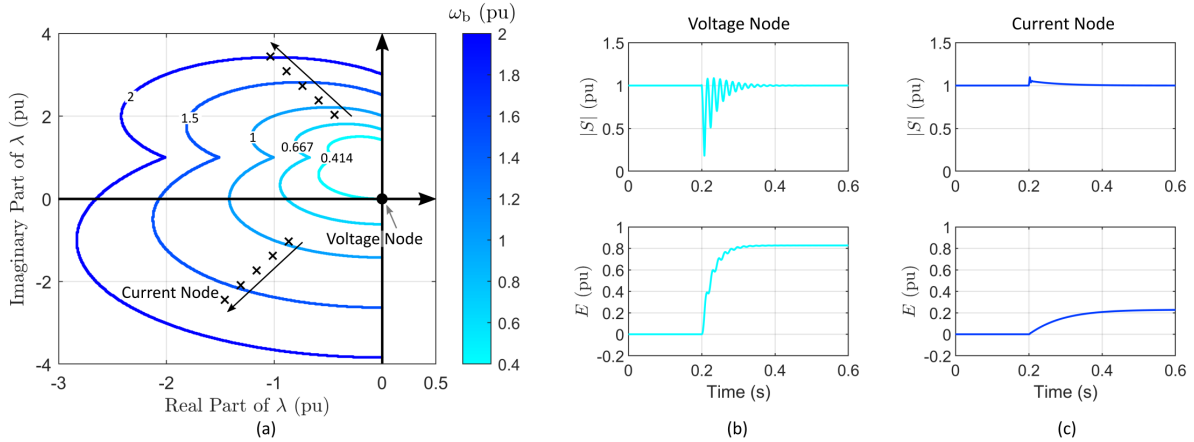


Fig. 4. Channel bandwidth and its impact on transient power. (a) Equi-bandwidth contour on the plane of channel eigenvalue indicating that current nodes have higher channel bandwidth ω_b than voltage nodes. (b)-(c) Transient power ($|S|$) and the accumulated energy (E) at a node subject to a phase jump at the remote end: (b) for a voltage node and (c) for a current node. The relatively low channel bandwidth associated to a voltage node results in high accumulated energy and requires a large energy cache. Some variables in the figure are presented per-unit (pu), and the details of the pu system is explained in Methods.

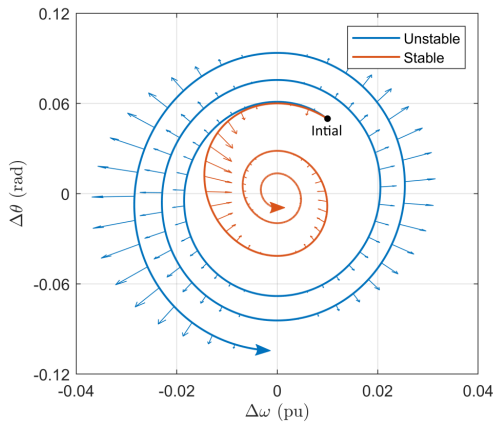


Fig. 5. Dynamic frequency shift may induce negative damping (shown as the outward arrow on the blue trajectory) of synchronisation dynamics. This needs to be stabilised by extra positive damping (shown as the inward arrow on the amber trajectory) in synchronisation control.

a unified synchronisation principle and it can be described by the simple formula below

$$H\dot{\omega} = W^* - W, \quad W = \text{Re}(e^{-j\mu} S) \quad (9)$$

where H is named *generalised inertia*, W is named *generalised power*, W^* is the reference value of W , μ is the angle of the axis to which S is projected into W , and ω is the angular frequency of the oscillator. If $\mu = 0$, $W = P$; if $\mu = \pi/2$, $W = Q$. The projection angle μ can be re-oriented to other values to create new synchronisation schemes for enhanced synchronisation stability. Detailed descriptions are included in Methods.

Rethinking Synchronising Stability

The power-communication isomorphism theory provides a new perspective to rethink power system stability. The theory may cover all aspects of power system stability, but we focus on synchronisation in this paper due to its fundamental importance explained in the previous section. In the synchronisation analysis, the amplitude of all signals are assumed constant, so the amplitude-angle modulation reduces to angle modulation. Now

we present the new insights into power system stability from the new theory.

First, the channel bandwidth determines the maximum speed of synchronisation among all nodes in the network. This also determines the maximum speed of power flow control over the network according to power-communication isomorphism. The channel bandwidth ω_b is determined by the eigenvalue λ of the channel. There are four types of channels in a network, namely voltage-voltage, voltage-current, current-voltage, current-current channels. A voltage-voltage channel is the channel between two voltage nodes, and other types are defined similarly. A voltage-voltage channel is generally an inductive transmission line with a very small resistance, so its eigenvalue is approximately zero and the corresponding channel bandwidth is $0.41\omega_0$ (ω_0 of the power system of 50 or 60 Hz). Other channels where current nodes are associated (i.e., voltage-current, current-voltage, and current-current channels) have a positive-real eigenvalue so their channel bandwidths are higher, as marked in Fig. 4 (a). This is because the parallel connected passive loads and the current control loops induce equivalent shunt resistances at the current node which reshapes the channel eigenvalue. Due to the relatively low channel bandwidth compared to a current node, a voltage node has a low power control speed, which results in high transient power and energy perturbation, as shown in Fig. 4 (b) and (c). The transient power perturbation is accumulated by the local energy cache (e.g. the dc-link capacitor), and hence a large energy cache is needed for a voltage node to suppress overshoot (e.g. the overshoot of dc-link voltage).

Second, the dynamic frequency shift of channels may induce negative damping in synchronisation stability. Combining the model of power-communication isomorphism in Fig. 1 and the unified synchronisation principle in (9), we get the whole-system synchronisation model. For any node (either current or voltage node) in the power system, its synchronisation with other nodes is governed by

$$H_m\dot{\omega}_m = W_m^* - \underbrace{\text{Re} \left(e^{-j\mu_m} \sum_n g_{mn} e^{j\vartheta_n} e^{j\vartheta_m^*} \right)}_{W_m}. \quad (10)$$

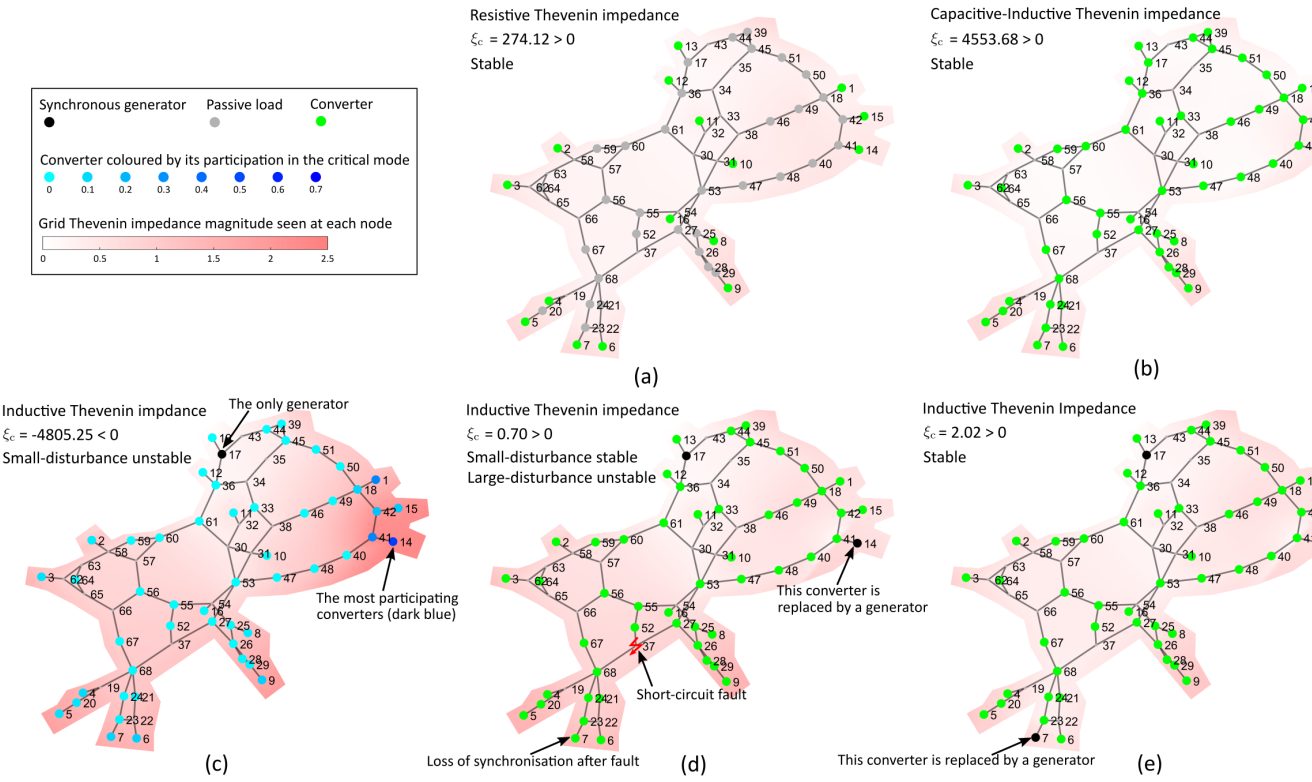


Fig. 6. Summary of test results on the IEEE 68-bus system. (a) 100% converters (grid-following) with passive loads. (b) 100% converters with active loads. (c) One synchronous generator (at node 17). (d) Two synchronous generators (at node 14,17). (e) Three synchronous generators (at node 7,14,17).

If the synchronisation dynamics is kept within the channel bandwidth, the channel gain is approximated by $g_{mn} \approx G_{mn}(\varpi_n) = G_{mn}(j\omega_n)$ which is a function of ω_n . Since W_m contains g_{mn} , W_m is also a function of ω_n . This power-frequency dependency, quantified by $\partial W_m / \partial \omega_n$, tends to be negative in many conditions, which induces negative damping in synchronisation dynamics and makes the system unstable, as illustrated in Fig. 5. This channel-induced negative damping should be compensated by extra positive damping in synchronisation control.

Lastly, we demonstrate that a power system with 100% grid-following converters can be well synchronised and thus stabilised, which was generally considered impossible. If sufficient damping are provided in synchronisation control, the frequency shift effect can be neglected by assuming $g_{mn} \approx G_{mn}(j\omega_0)$ is constant, and the synchronisation equation (10) becomes

$$H_m \dot{\omega}_m = W_m^* - \underbrace{D_m(\omega_m - \omega_0)}_{\text{Generalised Damping}} - \underbrace{\sum_n \Gamma_{mn} \sin(\theta_m - \theta_n + \gamma_{mn})}_{W_m} \quad (11)$$

where D_m is the generalised (active and reactive) damping coefficient, $\Gamma_{mn} = |g_{mn} A_m A_n|$, and $\gamma_{mn} = \pi/2 + \mu_m - \arg g_{mn}$. Equation (11) has interesting properties. The synchronisation coefficient Γ_{mn} is symmetric ($\Gamma_{mn} = \Gamma_{nm}$) due to the reciprocity of electrical networks. The phase offset γ_{mn} is dependent on network topology. In the following two conditions, γ_{mn} is approximately zero for $m \neq n$: (i) synchronisation of grid-forming apparatuses via inductive transmission lines; and (ii) synchronisation of grid-following inverters via shunt resistances (passive loads). In such cases, the synchronisation equation (11)

is reduced to a second-order Kuramoto model which has a wide stability region [16]. This implies that grid-following converters may have guaranteed synchronisation stability that is similar to grid-forming apparatuses.

In other cases where there are grid-forming and grid-following apparatuses co-exist, or where the power network is not purely inductive or resistive, $\gamma_{mn} \neq 0$, and the synchronisation pattern is more complicated. We can use linearisation method to evaluate the stability subject to small disturbances. Define $K_{mn} \triangleq \partial W_m / \partial \theta_n$ and $[K_H] \triangleq [H]^{-1}[K]$, where $[\cdot]$ denotes a matrix or a vector, $[K]$ is the matrix of K_{mn} , and $[H]$ is the diagonal matrix of H_m . $[K_H]$ is an extension of the synchronising power coefficients in conventional power systems, and therefore can be used as a generalised stability index. The eigenvalue of $[K_H]$ determines the small-disturbance stability of (11), and the eigenvector determines the modal participation. We define the critical eigenvalue ξ_c as the none-zero eigenvalue of $[K_H]$ that has the minimum real part. The system is small-disturbance stable if ξ_c has a positive real part.

We verified our theoretic findings on the IEEE 68-bus system, and the test results are summarised in Fig. 6. We tested five cases with different proportions of grid-following converters, subject to small and large disturbances. Tests (a)-(b) contain 100% grid-following converters with passive and active loads, and are stable under both small and large disturbances. We gradually replaced the converters by synchronous generators in tests (c)-(e), and found more complicated stability patterns. These agree well with the prediction of our theory. The critical eigenvalue ξ_c of $[K_H]$ provides accurate indication of small-disturbance stability in all cases. We also display in test (c) the participation

of each node in the critical eigenvalue, to show how $[K_H]$ helps to trace the root-cause of instability.

It is rather surprising to see that a power system with 100% converters (grid-following) is rather stable and recovers rather fast after faults (see Methods for the transient trajectories). It is even more surprising to see that adding a synchronous generator to the all-converter network destabilises the system, until more synchronous generators are added, which contradicts the conventional observation that synchronous generators are always helpful for grid stability. This phenomenon can be explained by the asymmetry of synchronisation between voltage nodes and current nodes, that is, it is more stable for current nodes to synchronise to voltage nodes than the opposite (see methods for details). This raises the important issue about the placement of grid-forming apparatuses in a converter dominated grid. We use two techniques to guide this placement: (i) participation analysis for the critical eigenvalue for small-disturbance stability, and loss of synchronisation analysis via time-domain simulation for large-disturbance analysis. These techniques are effective as verified in tests (c)-(d)-(e), showing succeeding improvements of stability when synchronous generators are placed at the identified nodes (14 and 7).

Grid impedances have significant impacts on the synchronisation stability. We coloured the grid map in Fig. 6 by the magnitude of the Thevenin impedance seen at each node. It is clear that small impedances tend to enhance stability. The grid impedances are resistive for case (a), capacitive-inductive (i.e., some nodes see capacitive Thevenin impedances, and others see inductive) for case (b), and inductive for case (c)-(e), because the impedances are shaped by passive loads, shunt capacitances, and transmission lines respectively. These impedance characteristics play important roles in the synchronisation stability of the corresponding cases, as explained in Methods.

Discussions

The power-communication isomorphism theory reveals the intrinsic resemblance of power systems and communication systems. This resemblance (isomorphism) shed lights into the stability of power systems from a communication perspective. The channel bandwidth determines the limit speed of synchronisation, and the channel-frequency dependency induces negative damping in synchronisation dynamics. These new findings provide new guidelines on the configuration of local energy cache and damping control. Based on the power-communication isomorphism, the power-based and signal-based synchronisation schemes are unified into a common principle. The unified synchronisation principle yields a surprising corollary that a power system with 100% grid-following converters can be well synchronised and thus stabilised, which was believed impossible. The unified synchronisation principle also creates simple stability indices for the assessment and enhancement of the synchronisation stability of complex power networks. All major findings are verified and demonstrated on the IEEE 68-bus test bench.

Methods

Technological Details. We present the technological details of power systems and communication systems to further illuminate the power-communication isomorphism. We start from describing the modulation and demodulation in communication

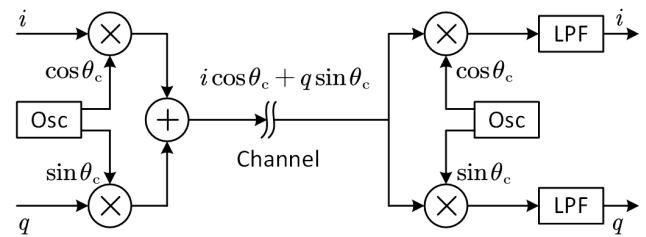


Fig. 7. Quadrature modulation-demodulation in communication systems.

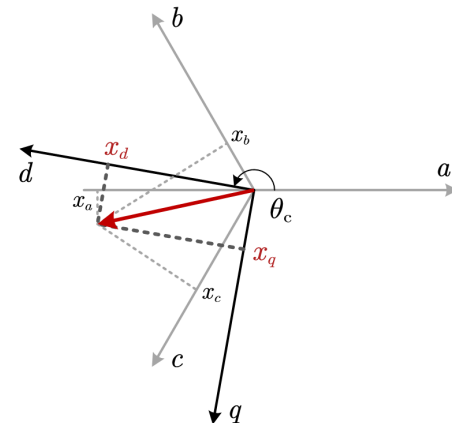


Fig. 8. The frame transformation in power systems that has an equivalent effect of modulation and demodulation.

systems. It is well known that there are three major modulation techniques in communication systems, that is, amplitude modulation, frequency modulation, and phase modulation. The frequency and phase modulation are often combined as angle modulation. All these three modulation techniques can be described as quadrature modulation, which is sketched in Fig. 7 [17]. The quadrature modulation contains two quadrature carriers, $\cos \theta_c$ and $\sin \theta_c$, where θ_c is the carrier angle generated by the integration of carrier frequency ω_c , that is $\theta_c = \int \omega_c dt$. The carriers are multiplied on the corresponding base-band signals i and q to create the modulated signal

$$x = i \cos \theta_c + q \sin \theta_c. \quad (12)$$

The signal x is transmitted over the channel and demodulated at the receiving end. In the demodulation, x is again multiplied by the quadrature carriers and passed through a low-pass filter (LPF) to restore the base-band signal. For example, $x \cos \theta = (i + i \cos 2\theta_c + q \sin 2\theta_c)/2$ contains a base-band signal $i/2$ and a double-carrier-band signal $(i \cos 2\theta_c + q \sin 2\theta_c)/2$ that is removed by the LPF to restore $i/2$. To avoid the LPF from distorting the base-band signal, the bandwidth of the base-band should be much smaller than the carrier frequency, which is known as the narrow-band condition [18].

Now we turn to power systems. The signals (voltages and currents) in power systems are generated in a rotating frame (either physical rotation of machinery or synthesised rotation in algorithm) [2]. The rotating frame contains two axes, which are called direct-quadrature (dq) axes. The signals in the dq frame form a vector (x_d, x_q) which maps to the three-phase signals

(x_a, x_b, x_c) via frame transformation, as illustrated in Fig. 8

$$x_a = x_d \cos \theta_c - x_q \sin \theta_c \quad (13)$$

where x_a is the a -phase signal, and θ_c is the angle displacement between the d axis and a phase (x_b and x_c follow similar transformations to x_a). It is clear that the frame transformation has a similar effect to quadrature modulation: (x_d, x_q) is equivalent to the base-band signal (i, q) and the rotating frequency of the dq frame is equivalent to the carrier frequency. A three-phase power system has two independent circuits which serve as two orthogonal communication channels. Therefore, the signals in the power system can be represented as a complex number with the real and imaginary parts each represent a channel [19]:

$$x_\alpha + jx_\beta = (x_d + jx_q)e^{j\theta_c} \quad (14)$$

where α and β represent the two orthogonal channels, $x_\alpha + jx_\beta$ is the modulated signal, $x_d + jx_q$ is the base-band signal, and $e^{j\theta_c} = \cos \theta_c + j \sin \theta_c$ is the carrier, all represented as complex numbers. Such a representation simplifies the quadrature modulation as complex-number multiplication, and the demodulation as the inverse multiplication

$$x_d + jx_q = (x_\alpha + jx_\beta)e^{-j\theta_c}. \quad (15)$$

It is clear that the demodulation on the orthogonal channels does not induce the extra double-carrier-frequency signal as in the single-channel modulation. As a result, no extra LPFs are needed after demodulation so the narrow-band condition can be relaxed. This allows for wide-band signals that may have more complicated interaction with channels, as discussed previously in the paper.

The quadrature signals can also be represented in polar coordinates

$$x_\alpha + jx_\beta = A e^{j(\theta_c + \phi)} = A \exp \left(j \int \omega_c dt + j\phi \right) \quad (16)$$

where $A = |x_d + jx_q|$ and $\phi = \arg(x_d + jx_q)$ are the amplitude and phase of the modulated signal respectively, and ω_c is the carrier frequency. The variation of (A, ϕ, ω_c) reflects amplitude, phase, and frequency modulation. In a grid-forming apparatus, A is constant and ϕ is zero, so only frequency modulation takes effect. In a grid-following converter, A and ϕ are used to control active and reactive power respectively, and ω_c follows the PLL [4], so the amplitude-phase-frequency modulation is all effective.

Mathematical Details. Some of the equations and conclusions in the paper are given without detailed explanations, which we provide here.

Firstly, we describe how the channel bandwidth equations (5)-(6) are obtained. Applying angle perturbations on both end of the channel g_{mn} , the corresponding complex power perturbation is

$$\Delta S_{mn} = S_{mn0}(\Delta\vartheta_m^* + \Delta\vartheta_n + g_{mn0}^{-1}\Delta g_{mn}). \quad (17)$$

Linearising the channel gain equation (4) yields

$$d\Delta g/dt = (\lambda - \varpi_0)\Delta g - g_0\Delta\varpi \quad (18)$$

from which we get the transfer function from $\Delta\varpi$ to Δg

$$\Delta g(s) = -\frac{g_0}{s + \varpi_0 - \lambda}\Delta\varpi(s). \quad (19)$$

Therefore,

$$g_{mn0}^{-1}\Delta g_{mn}(s) = \frac{-\Delta\varpi_n(s)}{s + \varpi_0 - \lambda} = \frac{-s\Delta\vartheta_n(s)}{s + \varpi_0 - \lambda}. \quad (20)$$

Putting this into (17) and noting that $\varpi_0 = j\omega_0$ (since the signal amplitude is constant in steady-state), we get the equations (5)-(6).

Secondly we prove the unified synchronisation principle in (9). The synchronisation of grid-forming apparatuses is governed by a physical or virtual inertia J

$$J\dot{\omega} = P^* - P \quad (21)$$

which apparently agrees with (9) if we defined $H = J$ and $W = P$. The synchronisation of a grid-following converter is governed by a PLL

$$\dot{\omega} = K_{\text{PLL}} v_q \quad (22)$$

where ω is the PLL internal frequency, K_{PLL} is the integral gain, and v_q is the q -axis voltage measured in the internal dq frame of the PLL. We have neglected the proportional control gain in (22) as this does not affect the essence of what we are illustrating. From the perspective of power-communication isomorphism, the dq current is modulated into the transmitted signal $e^{\vartheta_{\text{tx}}}$, and the dq voltage is demodulated from the received signal $e^{\vartheta_{\text{rx}}}$, that is

$$\begin{aligned} e^{\vartheta_{\text{tx}}} &= (i_d + j i_q) e^{j\theta_c} \\ v_d + j v_q &= e^{\vartheta_{\text{rx}}} e^{-j\theta_c} \end{aligned} \quad (23)$$

where $\theta_c = \int \omega dt$ is the PLL angle that serves as the carrier angle. Invoking the definition of the complex power in (2), we have

$$\begin{aligned} S &= e^{\vartheta_{\text{tx}}} e^{\vartheta_{\text{tx}}^*} = (v_d + j v_q)(i_d - j i_q) \\ &= \underbrace{i_d v_d + i_q v_q}_P + j \underbrace{(i_d v_q - i_q v_d)}_Q. \end{aligned} \quad (24)$$

Equation (22) can be rewritten as

$$\underbrace{i_d K_{\text{PLL}}^{-1}}_H \dot{\omega} = i_d v_q = \underbrace{i_q v_d}_W - \underbrace{(i_q v_d - i_d v_q)}_{W=-Q}. \quad (25)$$

This equation agrees with (9) if we define $H = i_d K_{\text{PLL}}^{-1}$, $W^* = i_q v_d$, and $W = -Q$. If the converter is absorbing power (i.e. an active load), $i_d < 0$, and the corresponding inertia H is negative. This can be avoided by defining $H = -i_d K_{\text{PLL}}^{-1}$, $W^* = -i_q v_d$, and $W = Q$. Thus we proved the unified synchronisation law.

Thirdly, we illustrate the impact of network impedance on synchronisation stability. The network impedance affects the channel gain g_{mn} and thus affects Γ_{mn} and γ_{mn} in the synchronisation equation (11). Taking a two-node system as an example, the synchronisation equations are

$$H\dot{\omega}_1 = W_1^* - \Gamma_{11} \sin(\gamma_{11}) - \Gamma_{12} \sin(\theta_1 - \theta_2 + \gamma_{12}) \quad (26)$$

$$H\dot{\omega}_2 = W_2^* - \Gamma_{22} \sin(\gamma_{22}) - \Gamma_{21} \sin(\theta_2 - \theta_1 + \gamma_{21})$$

where we assume the generalised inertias of the two nodes are identical and the dampings are neglected. The two-node synchronisation can be investigated by taking the difference of the two equations in (26)

$$H_\delta \dot{\omega}_\delta = W_\delta^* - \underbrace{\Gamma_\delta \sin(\delta + \gamma_\delta)}_{W_\delta} \quad (27)$$

TABLE I
CHANNEL GAINS AND THE ASSOCIATED SYNCHRONISATION PARAMETERS FOR THE CASES IN FIG. 9

Case	g_{11}	g_{22}	g_{12}	g_{21}	μ_1	μ_2	Γ_{mn}	γ_{11}	γ_{12}	γ_{21}	γ_{22}	Γ_δ	γ_δ	W_δ^*
(a)	$e^{-j\varphi}/Z$	$e^{j(\pi-\varphi)}/Z$	0	0			V^2/Z	$\frac{\pi}{2} + \varphi$	$\varphi - \frac{\pi}{2}$	$\varphi - \frac{\pi}{2}$	$\frac{\pi}{2} + \varphi$	$\sin \varphi V^2/Z$	0	P^*
(b)		$Ze^{j\varphi}$	$-\frac{\pi}{2}$	$-\frac{\pi}{2}$			I^2Z	$-\varphi$	$-\varphi$	$-\varphi$	$-\varphi$	$\cos \varphi I^2Z$	0	Q^*
(c)		$Ze^{j\varphi}$	$-\frac{\pi}{2}$	$\frac{\pi}{2}$			I^2Z	$-\varphi$	$-\varphi$	$\pi - \varphi$	$\pi - \varphi$	$\sin \varphi I^2Z$	$-\frac{\pi}{2}$	$\Gamma_\delta - Q^*$
(d)	jX	$\frac{-j}{X}$	1	-1	$-\frac{\pi}{2}$	0	See Note	$-\frac{\pi}{2}$	0	$-\frac{\pi}{2}$	π			Depends on H_1 and H_2

Note: For case (a), $W_1^* = -W_2^* = P^*$. For case (b)-(c), $W_1^* = -W_2^* = Q^*$. For case (d), $\Gamma_{11} = I^2X$, $\Gamma_{12} = V^2/X$, and $\Gamma_{21} = VI$.

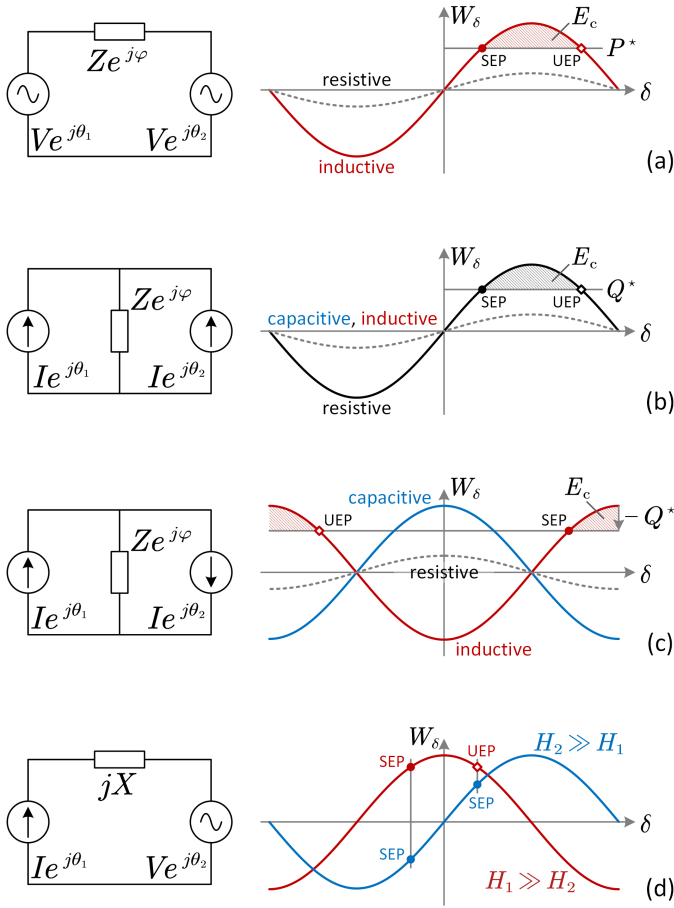


Fig. 9. The impact of grid impedance on the synchronisation between different types of nodes. (a) Synchronisation of two grid-forming apparatuses. (b) Synchronisation of two grid-following converters (sources). (c) Synchronisation of a grid-following source with a grid-following load (active load). (d) Asymmetry in synchronisation between current and voltage nodes.

where

$$\delta = \theta_1 - \theta_2, \quad \omega_\delta = \omega_1 - \omega_2 = \dot{\delta}, \quad H_\delta = H/2,$$

$$W_\delta^* = \frac{1}{2}(W_1^* - W_2^* + \Gamma_{22} \sin \gamma_{22} - \Gamma_{11} \sin \gamma_{11}), \quad (28)$$

$$\Gamma_\delta = \Gamma_{12} \cos \frac{1}{2}(\gamma_{12} + \gamma_{21}), \quad \gamma_\delta = \frac{1}{2}(\gamma_{12} - \gamma_{21}),$$

and we make use of the fact that $\Gamma_{12} = \Gamma_{21}$. We use (27) to examine the three cases in Fig. 9 (a)-(c), where two nodes are connected via impedance $Ze^{j\varphi}$ for power transmission. The channel gains and the associated synchronisation parameters for the three cases are listed in Table I. The W_δ is plotted against δ in Fig. 9 for different impedance angle φ . The intersection of

W_δ with W^* is the equilibrium point of synchronisation. Since W_δ is a sinusoidal function of δ , there might be two intersection points for $\delta \in (-\pi, \pi]$. The intersection point at the rising edge of W_δ is the stable equilibrium point (SEP), and the one at the falling edge of W_δ is the unstable equilibrium point (UEP). The area encircled by W_δ and W^* between the SEP and UEP is called the critical energy E_c , which defines the maximum transient energy that can be injected into the system without affecting synchronisation stability [20]. E_c is a reflection of the transient stability margin and is dependent upon the interconnection impedance $Ze^{j\varphi}$ between the two nodes. For case (a) in Fig. 9, E_c is highest if $Ze^{j\varphi}$ is inductive, and E_c reduces if $Ze^{j\varphi}$ changes from inductive to resistive (φ reduces from $\pi/2$ to 0), until there are no longer an SEP and the two nodes lose synchronisability at all. Fig. 9 (b) is similar to Fig. 9 (a) except that a resistive $Ze^{j\varphi}$ offers the highest E_c , and an inductive or capacitive $Ze^{j\varphi}$ reduces synchronisation stability. These two cases show that different impedance angles (representing channel phase shift) are preferred for the synchronisation of grid-forming and grid-following apparatuses. The synchronisation of grid-following converters is sensitive to the direction of power flow, as is clear to see from Fig. 9 (b)-(c). In Fig. 9 (c), one of the grid-following converters is changed from a source to a load, and the synchronisation pattern is significantly different, compared to Fig. 9 (b) where both converters are sources. The source-load synchronisation in Fig. 9 (c) prefers either an inductive or capacitive $Ze^{j\varphi}$, in contrast to the preference of resistive $Ze^{j\varphi}$ in Fig. 9 (b).

Fourthly, we discuss the asymmetry of synchronisation between a voltage node and a current node. The case is sketched in Fig. 9 (d), where a current node is connected to a voltage node via an inductive impedance jX . The corresponding channel gains and synchronisation parameters are given in Table I, and the synchronisation equations are

$$H_1 \dot{\omega}_1 = W_1^* + I^2 X - VI \sin \delta \quad (29)$$

$$H_2 \dot{\omega}_2 = W_2^* + VI \cos \delta$$

where $\delta = \theta_1 - \theta_2$. The synchronisation dynamics is dependent upon the ratio of H_1/H_2 . If $H_2 \gg H_1$, the voltage node has very high inertia so the current node synchronises to the voltage node. In such a case, $\dot{\omega}_2 \approx 0$ and $\dot{\omega}_\delta = \dot{\omega}_1 - \dot{\omega}_2 \approx \dot{\omega}_1$, so

$$H_1 \dot{\omega}_\delta = \underbrace{W_1^* + I^2 X}_{W_\delta^*} - \underbrace{VI \sin \delta}_{W_\delta} \quad (30)$$

If $H_1 \gg H_2$, the voltage node synchronise to a current node and the synchronisation equation becomes

$$H_2 \dot{\omega}_\delta = \underbrace{-W_2^*}_{W_\delta^*} - \underbrace{VI \cos \delta}_{W_\delta}. \quad (31)$$

The equations (30) and (31) represent very different synchronisation dynamics as is illustrated in Fig. 9 (d), which reflects asymmetry of synchronisation. Equation (30) corresponds to the blue curve and (31) corresponds to the red curve in Fig. 9 (d). Since the SEP of synchronisation must be on the rising edge of the W_δ curve, the two curves in Fig. 9 (d) have different stability ranges: $\delta \in (-\pi/2, \pi/2)$ for $H_2 \gg H_1$, and $\delta \in (-\pi, 0)$ for $H_1 \gg H_2$. In practice, δ operates within $(-\pi/2, \pi/2)$ which coincides with the stability range of $H_2 \gg H_1$, but $H_1 \gg H_2$ may become unstable for $\delta \in (0, \pi/2)$. As a result, $H_2 \gg H_1$ (current nodes synchronising to voltage nodes) is preferred over $H_1 \gg H_2$ (voltage nodes synchronising to current nodes). The asymmetry of voltage-current synchronisation helps to explain why test (c) is unstable but tests (d)-(e) gradually becomes stable in Fig. 6. The addition of further synchronous generators in tests (d)-(e) increase the total inertia of voltage nodes and thus enhances current-to-voltage synchronisation.

Lastly we explain why the eigenvalues of $[K_H]$ determine the local stability of (11). Linearising (11) yields

$$[\ddot{\Delta\theta}] = -[H]^{-1}[D][\dot{\Delta\theta}] - [K_H][\Delta\theta]. \quad (32)$$

where we make use of the fact that $[\Delta\omega] = [\dot{\Delta\theta}]$. The generalised inertia and damping are usually proportional, so we have $[H]^{-1}[D] = \sigma[I]$ where $[I]$ is a unit matrix and $\sigma = D_m/H_m$. Suppose that $[K_H]$ has not repeated eigenvalues, it can be diagonalised by similarity transformation $[K_H] = [\Phi][\Xi][\Phi]^{-1}$ where $[\Xi]$ is a diagonal matrix containing the eigenvalues of $[K_H]$, and $[\Phi]$ contains the corresponding eigenvectors. Define the coordinate transformation $[\Phi]^{-1}[\Delta\theta] = [z]$, and transform (32) to the z coordinate

$$[\ddot{z}] = -\sigma[\dot{z}] - [\Xi][z]. \quad (33)$$

Since $[\Xi]$ is diagonal, (33) reduces to a series of decoupled second order systems

$$\ddot{z}_m = -\sigma\dot{z}_m - \xi_m z_m \quad (34)$$

where $m \in \{1, 2, \dots, N\}$, N is the total number of nodes, and ξ_m is the m -th eigenvalue of K_H . The system (34) is stable if and only if its characteristic equation $s^2 + \sigma s + \xi_m = 0$ only has solutions in the left open half complex plane. We traverse s in the unstable right half plane to get the forbidden region of ξ_m , and the stable region is its complement

$$\text{Stable Region: } \{\xi_m \mid \text{Re } \xi_m > \sigma^{-2}(\text{Im } \xi_m)^2\}. \quad (35)$$

If sufficient damping is provided in synchronisation control, σ is large enough to render $\sigma^{-2}(\text{Im } \xi_m)^2$ very small, and the stability region is approximated by

$$\text{Stable Region: } \{\xi_m \mid \text{Re } \xi_m > 0\}. \quad (36)$$

All ξ_m must be within the stable region to ensure the synchronisation stability of the power system, with the only exception being the one that equals zero, which represents the collective spinning of the entire power system. Therefore we define the

critical eigenvalue ξ_c as the non-zero ξ_m (eigenvalue of $[K_H]$) that has the minimum real part.

Test Configurations and Results

The tested power system is built by modifying the standard IEEE 68-bus power system in Fig. 11. The IEEE 68-bus power system is a real-world system containing the interconnected New England Test System (NETS) and New York Power System (NYPS) [21]. This system has rich features and therefore is widely used in stability analysis. The buses in Fig. 11 are numbered in the same order as are the nodes in Fig. 6, and we use the terms “bus” and “node” interchangeably.

We replace the synchronous generators in the IEEE 68-bus system by grid-following converters to create a full converter system for test (a) in Fig. 6. We further replace the passive loads (resistive) by active loads (that is, loads that are interfaced by grid-following converters) for test (b). Tests (c)-(e) are configured by using synchronous generators to replace converters at nodes 17, 14 and 7 in succession.

Numerical simulation is conducted in Matlab/Simulink to generate the time-domain trajectories in Fig. 10. The grid-following converters used the full-order average model with an inner current loop, PLL, and harmonic filter. The current reference for the inner current loop is set to a constant value and no voltage saturation is implemented. The fourth-order model is used for synchronous generators which is a minimum model that preserves both electrical and mechanical dynamics.

All variables in this paper are presented in generator convention (also known as source convention, active sign convention), which defines the electric power flowing out of an apparatus as positive. Some variables are presented in per-unit (pu), which expresses a variable as normalised to a base value. The base values used are listed here: base frequency 60 Hz, base power 100 MVA, and base energy 1.67 MJ; the base energy equals the base power divided by the base frequency for consistency. The details of the the simulation models, code scripts, and system parameters used in this paper, are all available online at [22].

Finally, we present some interpretations of the simulation results in Fig. 10. The recovery from faults in Fig. 10 (a) [test (a) in Fig. 6] is very fast and this reflects the extended synchronisation stability of grid-following converters with passive loads. Fig. 10 (b) [test (b) in Fig. 6] shows angle swing after faults that are converged back to the equilibrium, which is similar to the angle swing of synchronous generators but is much faster, since the high channel bandwidth enables faster synchronisation. Excessive voltage overshoots are observed in this test, which is because the converters in our model do not implement voltage saturation. The voltage saturation may induce control logic switching and result in more complicated dynamics. Fig. 10 (c) [test (d) in Fig. 6] shows loss of synchronisation after faults from which we identified the most vulnerable node and guide the placement of grid-forming apparatuses. Fig. 10 (d) [test (e) in Fig. 6] is similar to Fig. 10 (b) but the voltage overshoot is much reduced because the additional synchronous generator clamps grid voltages and reduces the grid Thevenin impedances.

REFERENCES

[1] J. Bialek, “What does the GB power outage on 9 august 2019 tell us about the current state of decarbonised power systems?” *Energy Policy*, vol. 146, p. 111821, 2020.

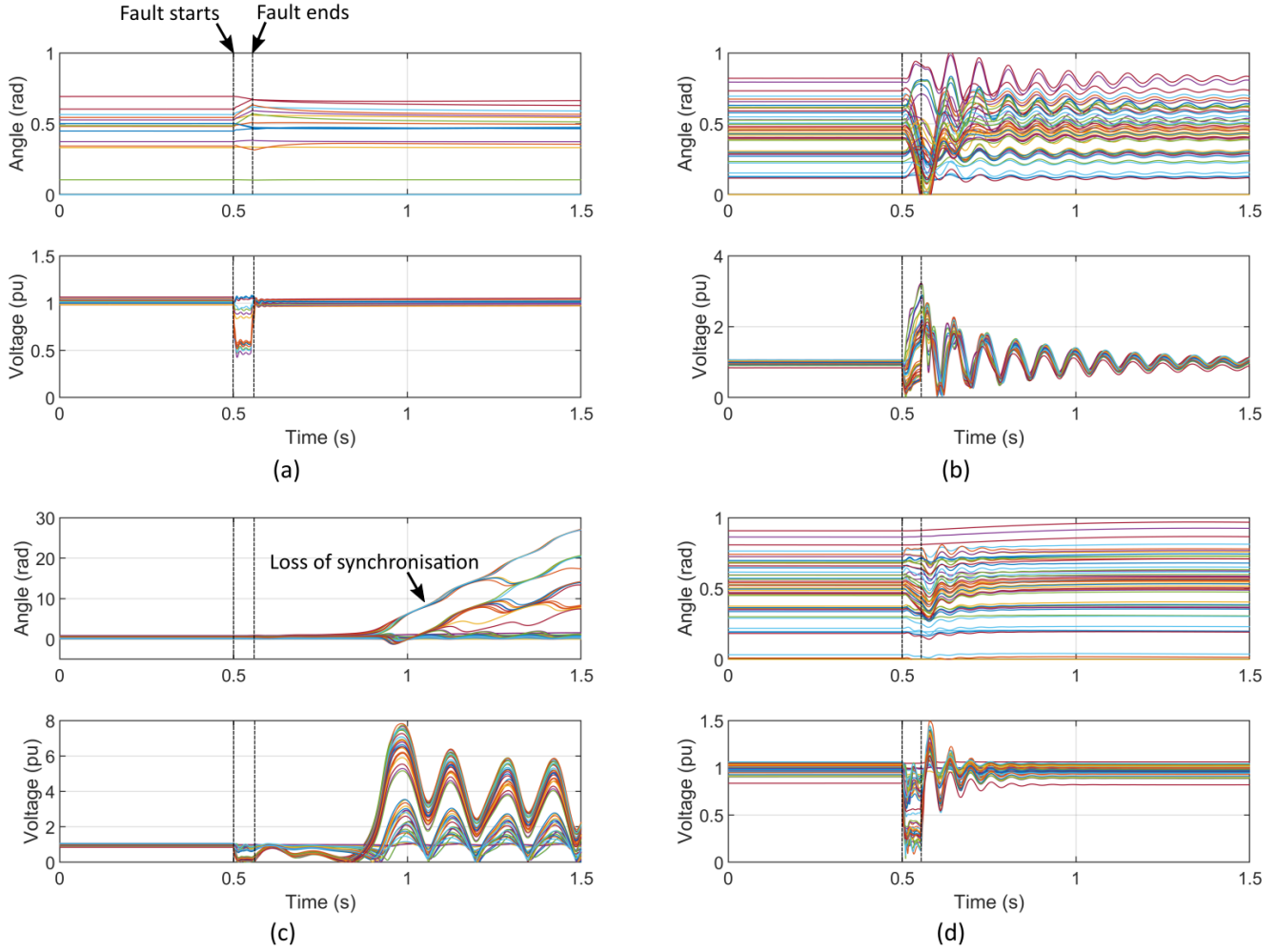


Fig. 10. Time-domain transient trajectories of the modified IEEE 68-bus system under a short-circuit fault, which occurs at bus 37 at 0.5 s and is cleared after 3 fundamental cycles, i.e., at 0.55 s. (a) 100% converters (grid-following) with passive loads. (b) 100% converters with active loads. (c) Two synchronous generators (at node 14,17). (d) Three synchronous generators (at node 7,14,17). The results in (a)-(d) corresponds to tests (a),(b),(d) and (e) in Fig. 6. The simulation result for test (c) is not stable around the equilibrium and is therefore not presented.

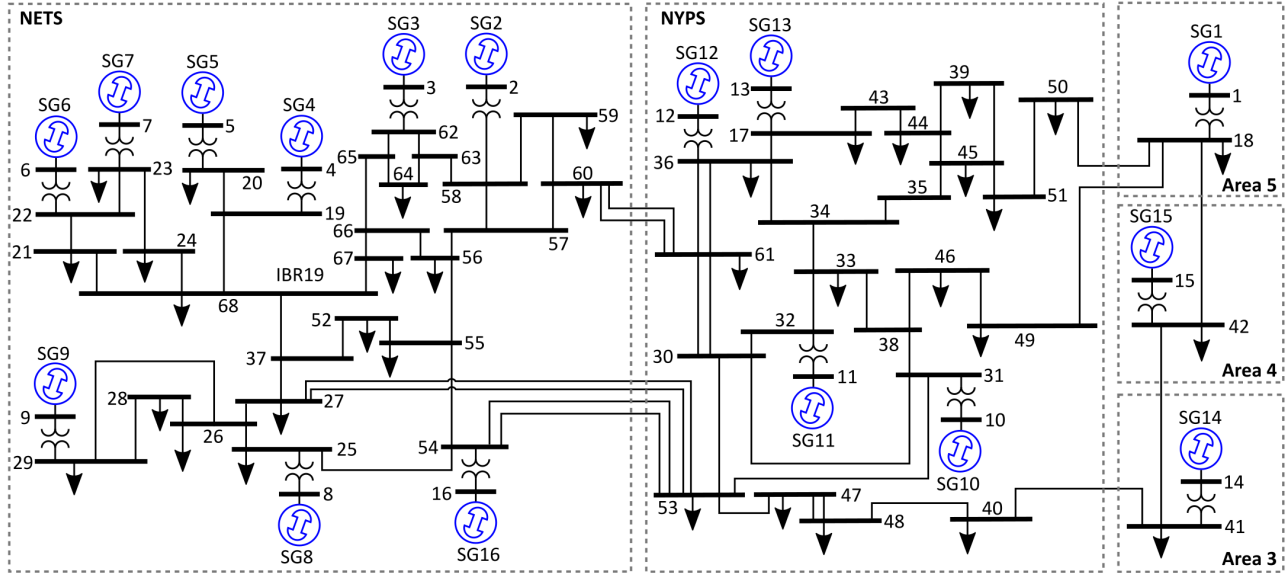


Fig. 11. Layout of the standard IEEE 68-bus NETS-NYPS power system. The system is modified by replacing synchronous generators with converters, and replacing passive loads with active loads in some cases. The configuration transmission lines, shunt commentator, and power flows are not changed.

- [2] P. Kundur, *Power system stability and control*. McGraw-hill New York, 1994, vol. 7.
- [3] P. Kundur *et al.*, “Definition and classification of power system stability ieee/cigre joint task force on stability terms and definitions,” *IEEE Trans. Power Syst.*, vol. 19, no. 3, pp. 1387–1401, 2004.
- [4] J. Rocabert, A. Luna, F. Blaabjerg, and P. Rodríguez, “Control of power converters in AC microgrids,” *IEEE Trans. Power Electron.*, vol. 27, no. 11, pp. 4734–4749, Nov. 2012.
- [5] S. O. Framework, “Performance of Phase-locked Loop based converters,” National Grid, Tech. Rep., 2018.
- [6] G. Wu, B. Zhao, X. Zhang, S. Wang, A. Egea-Álvarez, Y. Sun, Y. Li, D. Guo, and X. Zhou, “Impact of non-minimum-phase zeros on the weak-grid-tied VSC,” *IEEE Transactions on Sustainable Energy*, vol. 12, no. 2, pp. 1115–1126, 2020.
- [7] K. W. Martin, “Complex signal processing is not complex,” *IEEE Transactions on Circuits and Systems I: Regular Papers*, vol. 51, no. 9, pp. 1823–1836, 2004.
- [8] F. Briz, M. W. Degner, and R. D. Lorenz, “Analysis and design of current regulators using complex vectors,” *IEEE Transactions on Industry Applications*, vol. 36, no. 3, pp. 817–825, 2000.
- [9] D. Pattabiraman, R. Lasseter, and T. Jahns, “Comparison of grid following and grid forming control for a high inverter penetration power system,” in *2018 IEEE Power & Energy Society General Meeting (PESGM)*. IEEE, 2018, pp. 1–5.
- [10] L. S. Czarnecki, “On some misinterpretations of the instantaneous reactive power pq theory,” *IEEE transactions on power electronics*, vol. 19, no. 3, pp. 828–836, 2004.
- [11] M. V. Clark, “Adaptive frequency-domain equalization and diversity combining for broadband wireless communications,” *IEEE Journal on Selected Areas in Communications*, vol. 16, no. 8, pp. 1385–1395, 1998.
- [12] G. L. Stüber and G. L. Steuber, *Principles of mobile communication*. Springer, 1996, vol. 2.
- [13] A. Oppenheim, A. S. Willsky, and I. Young, “Signals and systems,” *Prentice-Hall, Englewood Cliffs, New Jersey*, vol. 19, pp. 146–153, 1983.
- [14] L. Zhang, L. Harnefors, and H.-P. Nee, “Power-synchronization control of grid-connected voltage-source converters,” *IEEE Transactions on Power systems*, vol. 25, no. 2, pp. 809–820, 2009.
- [15] S. D’Arco and J. A. Suul, “Equivalence of Virtual Synchronous Machines and Frequency-Droops for Converter-Based MicroGrids,” *IEEE Transactions on Smart Grid*, vol. 5, no. 1, pp. 394–395, Jan 2014.
- [16] J. Peng, “Synchronization in the second-order kuramoto model,” 2015.
- [17] L. Hanzo, S. X. Ng, W. Webb, and T. Keller, *Quadrature amplitude modulation: From basics to adaptive trellis-coded, turbo-equalised and space-time coded OFDM, CDMA and MC-CDMA systems*. IEEE Press-John Wiley, 2004.
- [18] G. Wade, *Signal coding and processing*. Cambridge university press, 1994.
- [19] Y. Li, Y. Gu, and T. C. Green, “Interpreting frame transformations in ac systems as diagonalization of harmonic transfer functions,” *IEEE Transactions on Circuits and Systems I: Regular Papers*, vol. 67, no. 7, pp. 2481–2491, 2020.
- [20] H.-D. Chiang and J. S. Thorp, “Stability regions of nonlinear dynamical systems: A constructive methodology,” *IEEE Transactions on Automatic Control*, vol. 34, no. 12, pp. 1229–1241, 1989.
- [21] C. Canizares, T. Fernandes, E. Gerald, L. Gerin-Lajoie, M. Gibbard, I. Hiskens, J. Kersulis, R. Kuiava, L. Lima, F. DeMarco *et al.*, “Benchmark models for the analysis and control of small-signal oscillatory dynamics in power systems,” *IEEE Transactions on Power Systems*, vol. 32, no. 1, pp. 715–722, 2016.
- [22] “Future Power Networks.” [Online]. Available: <https://github.com/Future-Power-Networks/Publications>